

MuPix and ATLASPix – Architectures and Results

A. Schöning^{*a}, J. Anders^b, H. Augustin^a, M. Benoit^c, N. Berger^d, S. Dittmeier^a, F. Ehrler^e, A. Fehr^b, T. Golling^c, S. Gonzalez Sevilla^c, J. Hammerich^{a†}, A. Herkert^a, L. Huth^{a‡}, G. Iacobucci^c, D. Immig^a, M. Kiehn^c, J. Kröger^f, F. Meier^{ag}, A. Meneses Gonzalez^a, A. Miucci^b, L.O.S. Nohte^a, I. Peric^e, M. Prathapan^e, T. Rudzki^a, R. Schimassek^e, D M S Sultan^c, L. Vigani^a, A. Weber^a, M. Weber^b, W. Wong^c, E. Zaffaroni^c, H. Zhang^h

^a *Physics Institute, Heidelberg University,
Im Neuenheimer Feld 226, 69120 Heidelberg, Germany*

^b *Physics Institute, University of Bern,
Sidlerstrasse 5, 3012 Bern, Switzerland*

^c *Department of Nuclear Physics, University of Geneva,
24, quai Ernest-Ansermet, CH-1211 Genève 4, Switzerland*

^d *Institute for Nuclear Physics, University of Mainz,
Johann-Joachim-Becher-Weg 45, 55128 Mainz*

^e *Institute of Data Processing and Electronics, Karlsruhe Institute of Technology,
P.O. Box 3640, 76021 Karlsruhe, Germany*

^f *Organisation Européenne pour la Recherche Nucléaire (CERN),
1211 Geneva 23, Switzerland*

^g *Paul-Scherrer Institute, Villigen,
Forschungsstrasse 111, 5232 Villigen, Switzerland
E-mail: schoning@physi.uni-heidelberg.de*

High Voltage Monolithic Active Pixel Sensors (HV-MAPS) are based on a commercial High Voltage CMOS process and collect charge by drift inside a reversely biased diode. HV-MAPS represent a promising technology for future pixel tracking detectors. Two recent developments are presented. The MuPix has a continuous readout and is being developed for the Mu3e experiment whereas the ATLASPix is being developed for LHC applications with a triggered readout. Both variants have a fully monolithic design including state machines, clock circuitries and serial drivers. Several prototypes and design variants were characterised in the lab and in testbeam campaigns to measure efficiencies, noise, time resolution and radiation tolerance. Results from recent MuPix and ATLASPix prototypes are presented and prospects for future improvements are discussed.

*The 28th International Workshop on Vertex Detectors - Vertex2019
13-18 October, 2019
Lopud, Croatia*

*Speaker.

†now at University of Liverpool, UK

‡now at DESY, Hamburg, Germany

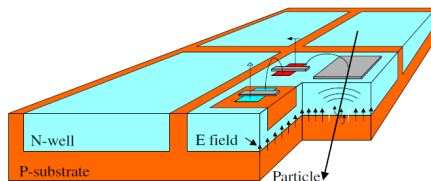


Figure 1: Schematic drawing of an HV-MAPS [1].

Future particle physics experiments have increasing demands concerning particle rates, time and spatial resolution, and radiation tolerance. For the construction of semiconductor trackers, monolithic active pixel sensors (MAPS) represent a very attractive alternative to standard hybrid designs where the sensors and readout chips are on different dies. Hybrid designs require interconnects like wires or bump bonds which are a limiting factor for the maximum achievable spatial resolution and the scalability when it comes to instrumenting large areas. Particularly interesting are depleted MAPS which collect ionisation charge mainly via drift, provide time resolutions of a few nanoseconds and are radiation tolerant.

1. High Voltage Monolithic Active Pixel Sensors (HV-MAPS)

In contrast to ordinary MAPS designs where the charge collecting diode and the pixel electronics are spatially separated, HV-MAPS exploit HV-CMOS processes and implement the pixel electronics inside a deep n-well [1]. HV-MAPS collect ionisation charge mainly via drift, see figure 1, and provide time resolutions of a few nanoseconds in contrast to standard MAPS which collect ionisation charge mainly by diffusion. The depletion depth grows with the bias voltage and the substrate resistivity. Breakdown voltages of up to 200 V have been realised, depending on the substrate resistivity and the electrical field in the pixels (e.g. guard ring design). The fast collection of the signal charges and the low noise allow for the implementation of continuous readout schemes where zero suppressed hits are only temporarily buffered and sent out using fast Gbit/s links.

HV-MAPS have been prototyped for several experiments (Mu3e, ATLAS, CLIC) with different readout architectures. HV-MAPS are also considered for other particle and nuclear physics experiments. All designs have in common that the readout circuitry is spatially separated from the active pixel matrix. They provide fast time stamping and charge measurement using time-over-threshold (ToT), thus allowing for timewalk correction. Due to the small size of the active depletion zone of about 15-50 μm for substrate resistivity of 20-200 Ωcm , HV-MAPS detectors can be thinned down to 50-100 μm . This makes the HV-MAPS concept interesting for low energy experiments like Mu3e, where charged particle tracking is limited by multiple scattering. For the silicon pixel detector of the Mu3e experiment [2], aiming to search for the decay $\mu^+ \rightarrow e^+e^+e^-$ with unprecedented sensitivity, the MuPix sensor is being developed.

The ATLASPix development, on the other hand, was originally intended to provide for the new ATLAS inner tracker system (ITk) at High Luminosity LHC an alternative sensor technology for the outermost pixel layer at a radius of 29 cm. Several HV-MAPS prototypes, submitted in a common engineering run in the year 2017, are shown in figure 2. In the following the focus is put on results obtained from MuPix8 (submatrix A) and ATLASPix1 (version *simple*) characterisation

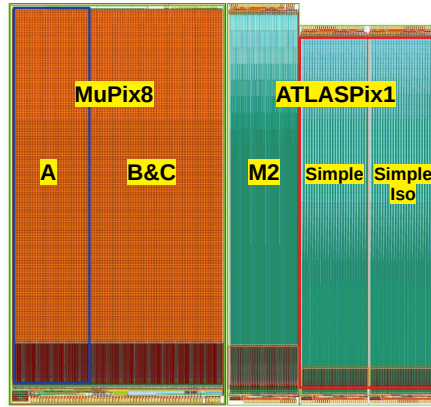


Figure 2: CAD views of MuPix8 and ATLASPix1 prototypes as produced on the same reticle.

studies. A main difference between the sensors is the way how signals are transferred from the active matrix to the periphery. All MuPix sensors amplify the collected charges in the pixel cell and send the amplified signal to the periphery where the comparators are located. The submatrix A of MuPix8 implements a source follower whereas submatrices B&C implement a current driver. All ATLASPix sensors have the comparators in the pixel cell and send the discriminated output to the periphery where the readout logic is implemented. The readout logic and state machine of MuPix8 and ATLASPix1_Simple are very similar and provide data streaming (continuous readout). ATLASPix1_M2 implements trigger buffers and is not discussed here. ATLASPix1 was produced in different flavours: In ATLASPix1_Simple the discriminator is realised in NMOS-logic whereas CMOS-logic is used in the ATLASPix1_Simple_Iso. An isolating deep p-well is implemented here to better shield the charge sensitive diode from the p-type transistors.

All prototypes discussed here have radiation tolerant designs, including the use of enclosed layout transistors where necessary. Signal collection in the diode is also radiation tolerant, since charge is collected over short drift lengths and not strongly affected by bulk damage.

The main specification parameters of the HV-MAPS sensors discussed in this talk are shown

	MuPix8	MuPix10	ATLASPix1_Simple	ATLASPix3
Process	AH18 (AMS) [3]	H18 (TSI) [4]	AH18 (AMS) [3]	H18 (TSI) [4]
Sensor size [mm ²]	10.7 × 19.5	20.2 × 23.0	3.4 × 18.4	20.2 × 21.0
Pixel matrix	128 × 200	250 × 256	25 × 400	132 × 372
Pixel size [μm ²]	81 × 80	80 × 80	130 × 40	150 × 50
Active area [mm ²]	10.3 × 16.0	20.1 × 20.0	3.25 × 16.0	19.8 × 18.6
#Bits timestamp & ToT	10+6	11+5	10+6	10+7
Pixel tune DACs [bits]	3	3	3	3
Bandwidth [Gbit/s]	≤ 1.6 (3×)	≤ 1.6 (3×)	≤ 1.6	1.28
Readout architecture	continuous	continuous	continuous	trigger (cont.)
Status (December 2019)	tested	in production	tested	under test

Table 1: Main specification parameters of the HV-MAPS sensors discussed in this talk.

in table 1. The MuPix8 and ATLASPix1_Simple sensors were produced in the AH18 (180 nm) HV-CMOS process by ams AG (AMS) [3] and have been fully characterised in the lab and in several test beams at CERN, DESY, FERMILAB and PSI.

2. MuPix Design and Results

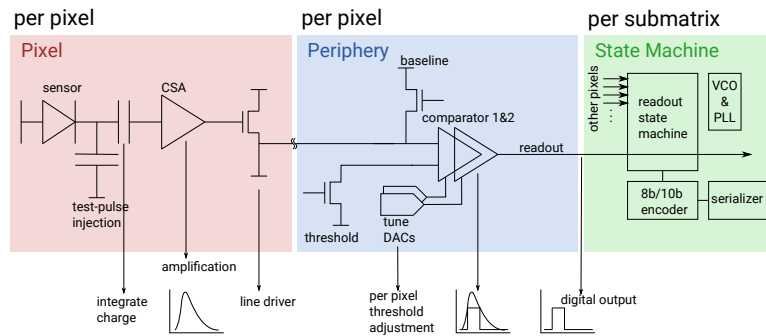


Figure 3: Schematics of the MuPix8 readout.

All MuPix prototypes implement the amplifier in the active pixel cell and the comparator in the periphery, both interconnected by an analogue readout line. The periphery of all recent prototypes contains in addition: readout buffers, the state machine, PLL and VCO, 8/10 bit encoders, and serializers providing data output rates of up to 1.6 Gbit/s per link, see figure 3.

The MuPix8 features two comparators per pixel which allow for different operation modes for timewalk correction and mitigation. The 2-threshold method mitigates timewalk by using a very low threshold for time stamping and a higher threshold for hit validation, see figure 4. This allows the sensor to operate with low noise (high threshold) and low jitter (low threshold). In addition, timewalk can be corrected offline by exploiting the 6-bit ToT information. Results of time resolution measurements are discussed in section 4.

Efficiency and noise have been measured in test beams as a function of the comparator threshold. Figure 5a shows the results obtained for a MuPix8 sensor produced with a substrate resistivity of 80 Ωcm . A plateau of high efficiency is reached for thresholds below 80 mV. For higher thresh-

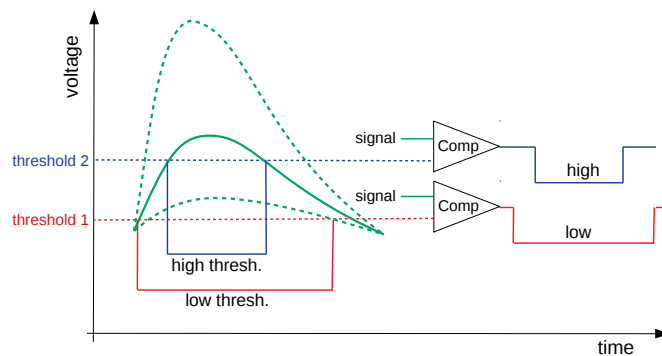


Figure 4: The 2-threshold concept of MuPix8.

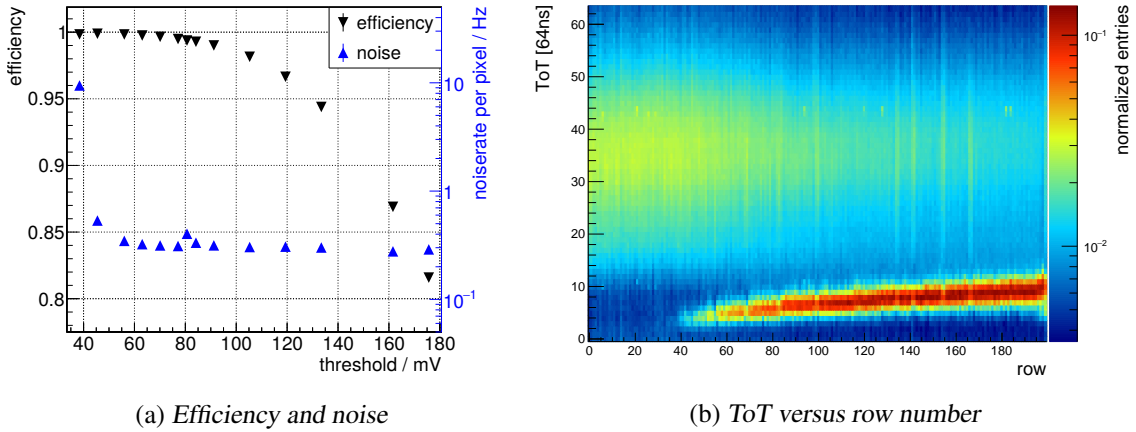


Figure 5: *Left: Efficiency and noise of MuPix8 with a substrate resistivity of 80 Ωcm as function of the threshold voltage. A threshold of 100 mV corresponds to about $1350e^-$. Right: ToT distribution (normalised) as function of the pixel row number. Plots taken from [8, 9].*

olds, inefficiencies arise from charge sharing effects at pixel edges and corners. For thresholds above 50 mV the noise rate is very low and significantly below 1 Hz per pixel. For thresholds below 50 mV the noise rate significantly increases. In the range 50-80 mV a stable operation of MuPix8 is possible, providing high efficiency above 99% at low noise.

A disadvantage of the MuPix8 design are the long interconnects between active pixel matrix and periphery of up to 2 cm length which cause large interline capacitances. The resulting cross talk crucially depends on the spacing of the readout lines. The MuPix8 sensor has six metal layers and uses two for signal lines. Measurements have shown significant cross talk which slightly compromises the hit detection efficiency for pixels with long routings. The cross talk between the interconnects can be seen in figure 5b which shows the ToT distribution as function of the row number of the pixel. For small row numbers (short interconnects) a signal peak is visible for ToT= 35. For row numbers ≥ 40 a second peak appears originating from cross talk.

3. ATLASPix

An alternative readout architecture which implements the comparator in the pixel cell has been developed for ATLAS at LHC. This architecture is practically immune against cross talk from interline capacitances and has the advantage that the signal is discriminated just after amplification, and thus not deteriorated by driving the analogue signal over long lines like in the MuPix design. A disadvantage is the larger pixel capacitance from the comparator logic inside the pixel cell.

First results from ATLASPix1 characterisation studies at CERN and FERMILAB have been reported in [5, 6]. More results were obtained at recent test beam campaigns at DESY and PSI. Single hit efficiencies have been measured and are shown in figure 6 for samples with substrate resistivities of 80 Ωcm and 200 Ωcm as a function of the discriminator threshold and different bias voltages. For bias voltages above 50 V a high efficiency plateau is visible for a threshold range of 50-100 (50-200) mV for substrate resistivities of 80 (200) Ωcm . For bias voltages of 70-80 V single hit efficiencies exceeding 99.7% are reached with practically negligible noise rates.

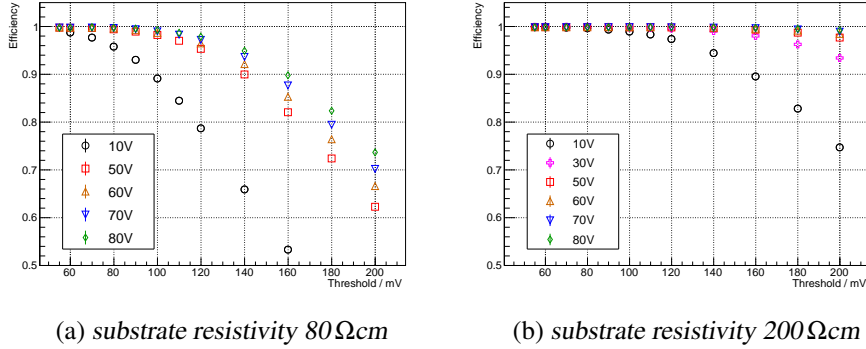


Figure 6: Single hit efficiencies of ATLASPix1_Simple for two different substrate resistivities as function of the discriminator threshold and for different bias voltages. The measurement were performed with pions of 300 MeV/c at the PSI testbeam. Plots taken from [7].

4. Time Resolution

The time resolutions of the MuPix8 and ATLASPix1 sensors are measured with a ^{90}Sr source. For MuPix8, the measurement is performed for different operation modes of the two comparators (see section 2). Operating the sensor using a common comparator threshold of 50 mV, corresponding to about $650 e^-$, a time resolution of 7.6 ns (10.5 ns) is measured with (w/o) timewalk correction. Using the 2-threshold method with a lower threshold at 35 mV, the time resolution improves to 6.7 ns (8.8 ns), respectively. The two-threshold method therefore helps to improve the time resolution, even if an offline timewalk correction is applied.

For MuPix8, the map of time resolutions as function of the pixel region is shown in figure 7a for a common comparator threshold of 50 mV. A clear row dependence is visible: pixels at low row numbers have a better time resolution than those at large row numbers. This suggests that the large interconnects negatively affect the analogue pulses and the time resolution. However, an insufficient power distribution over the matrix can also not be excluded, given that power supply and bias signals originate from the periphery near the bottom row of the pixel matrix. Similar time resolution maps are shown in figures 7b and c for ATLASPix1_Simple and ATLASPix1_Simple_Iso, respectively. These distributions look much more homogeneous and for the latter there is no loss

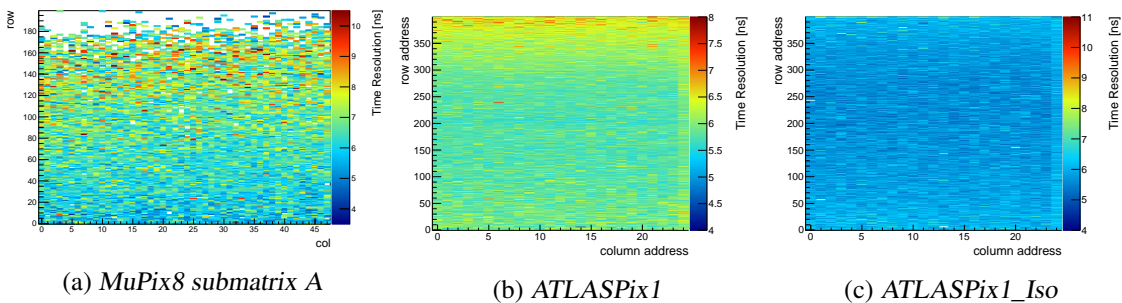


Figure 7: Maps of the time resolution of the full pixel matrix after timewalk correction as measured by a ^{90}Sr source with a reference timing counter. Plots from [8, 10].

	MuPix8	ATLASPix1	
		Simple	ISO p-well
Timestamp sampling [ns]	8.0	16.0	16.0
Time resolution (σ_{fit})			
- w/o TW correction [ns]	8.8	8.1	6.8
- with TW correction [ns]	6.7	5.9	5.8
- internal resolution [ns]	6.3	3.7	3.6

Table 2: Time resolution of the three different sensor types before and after timewalk (TW) correction using ToT information. The internal time resolution is defined by the TW-corrected resolution minus the quadratically subtracted sampling resolution given by the time stamping frequency.

of resolution with higher row numbers, which are further from the periphery.

A quantitative comparison of the time resolution obtained by MuPix8 with the 2-threshold method and both ATLASPix1_Simple versions which implement only one comparator threshold is given in table 2. All three sensors show very similar time resolutions after timewalk correction. However, integrating a different clock division scheme, the MuPix8 has a two times higher sampling frequency than both ATLASPix1 versions. Therefore, the time resolutions measured for ATLASPix1 include a significant component from the sampling. By correcting the sampling uncertainty an internal time resolution is calculated. This time resolution is ~ 3.7 ns for both ATLASPix1_simple versions and significantly lower than the 6.3 ns obtained for MuPix8.

5. Irradiation Studies

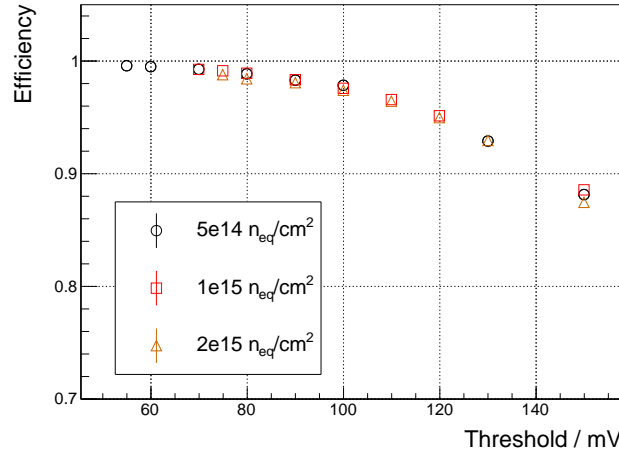


Figure 8: Single hit efficiency for neutron irradiated ATLASPix1_Simple with a substrate resistivity of $80 \Omega\text{cm}$ as function of the comparator threshold for fluences of $5 \cdot 10^{14}$, $1 \cdot 10^{15}$, and $2 \cdot 10^{15} n_{\text{eq}}/\text{cm}^2$. The sensors are thinned to $62 \mu\text{m}$ and a bias voltage of 60 V is applied. All sensors are untuned and had a temperature of about 5°C . Plot taken from [7].

The radiation hardness of the AMS H18 process has been investigated in previous works [11, 12] including an electrical characterisation of irradiated ATLASPix1 prototypes [13]. Single hit efficiencies for a fully monolithic HV-MAPS¹ irradiated with protons and neutrons were reported first for the MuPix7 predecessor [14] which has no radiation hard design. These performance studies have been repeated for the ATLASPix1_Simple prototype and first results were reported in [5]. Results from a more comprehensive study are summarized in the following.

Samples of ATLASPix1_Simple were irradiated with neutrons at the TRIGA Mark II research reactor in Ljubljana [15] and with 17 MeV protons at the Bern Cyclotron Laboratory [16]. Single hit efficiencies were measured in testbeams for various irradiated sensors with fluences up to several 10^{15} n_{eq}/cm² as function of the threshold and bias voltage. Figure 8 shows exemplarily a threshold scan for 80 Ωcm samples irradiated with neutrons for three fluences up to $2 \cdot 10^{15}$ n_{eq}/cm². All efficiency curves are very similar and show no significant loss of efficiency for higher fluences. However, differences are observed in the noise levels which increase with fluence; for fluences $\geq 10^{15}$ n_{eq}/cm², comparator thresholds of $\lesssim 50$ mV can only be reached by masking noisy pixels.

In order to compare the maximum achievable sensor efficiencies at similar noise levels, the most noisy pixels are excluded (masked) until a reasonable noise level is reached, i.e. when the average pixel noise is below 40 Hz, corresponding to a noise rate of 10^{-6} per pixel and LHC bunch crossing. All sensors were untuned, i.e. a common comparator threshold above noise was applied to all pixels. The resulting maximum efficiencies after neutron and proton irradiation are shown in table 3. All sensors show a high efficiency above 98% for fluences of up to $2 \cdot 10^{15}$ n_{eq}/cm² at high bias voltages of up to 80-85 V. The total ionising doses (TID) of the proton-irradiated sensors are here 10 MRad (48 MRad) for fluences of $1 \cdot 10^{14}$ ($5 \cdot 10^{14}$) n_{eq}/cm². Note that the sensor irradiated

Resistivity / Ωcm	Fluence / 10 ¹⁴ n _{eq} /cm ²	-60 V	-70 V	-80/85 V
		Efficiency / %		
80	1 (n)	96.3	97.5	98.3
	5 (n)	99.5	-	-
	10 (n)	99.3	-	99.5
	20 (n)	98.5	98.4	98.6
200	0	-	-	≥ 99.7
	5 (n)	99.2	-	-
	10 (n)	98.8	-	[†] 99.5
	20 (n)	96.5	-	98.7
	1 (p)	[†] 99.7		
	5 (p)	99.6	99.7	99.9

Table 3: Maximum efficiencies of proton (p) and neutron (n) irradiated ATLASPix1_Simple sensors at an average noise rate per pixel of $\lesssim 40$ Hz. The sensors with a wafer resistivity of 80 Ωcm are thinned to 62 μm, the 200 Ωcm to 100 μm, and the sensors where the efficiency is labeled with [†] have not been thinned (725 μm). Modified table from [7].

¹We define a pixel sensor as being fully monolithic if the full readout architecture including VCO, PLL and state machine is implemented.

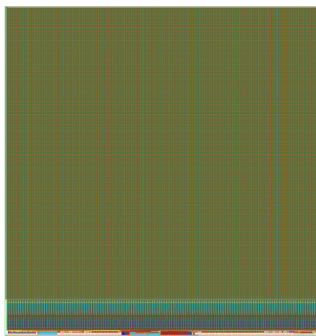
to a fluence of $1 \cdot 10^{14}$ n_{eq}/cm^2 has been biased during irradiation and was working perfectly.

6. Summary and Outlook

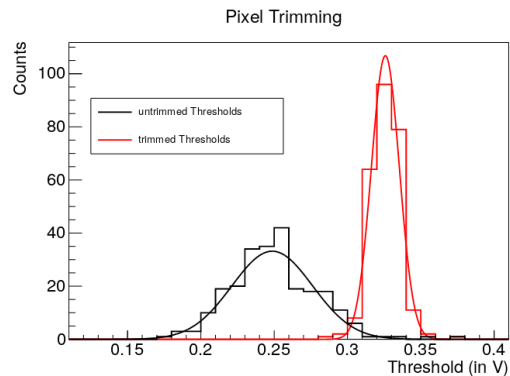
Several HV-MAPS prototypes for different experimental applications and with different read-out architectures have been developed in the last years. This talk focuses on two developments of fully monolithic pixel sensors: MuPix for the Mu3e experiment and ATLASPix for the outer pixel layer of the new ATLAS inner tracker. Results from characterisation studies are presented for the MuPix8 and ATLASPix1_Simple prototypes which have been produced in the ams AH18 process with different substrate resistivities (20-1000 Ωcm) and with different sensor thicknesses (50-725 μm). All prototypes show an excellent performance concerning efficiency and noise, even after irradiation with protons and neutrons with fluences of up to $2 \cdot 10^{15}$ n_{eq}/cm^2 . Time resolutions of about 6 ns are measured for MuPix8 and ATLASPix1_Simple after timewalk correction. Correcting for binning effects from the on-chip time stamping a chip-internal time resolution of ~ 3.7 ns is derived for ATLASPix1_Simple and ATLASPix1_Simple_Iso.

The very good time resolutions should be confirmed with the newest sensor, ATLASPix3, see figure 9a. It is designed to be functionally compatible to the RD53 readout chip [17] and was produced in the 180 nm process by TSI [4]. ATLASPix3 is the largest HV-MAPS sensor produced so far, see table 1, and was delivered in August 2019. ATLASPix3 is fully operational and a first result is shown in figure 9b. If the ongoing measurements follow its predecessor ATLASPix1 in terms of efficiency, noise, time resolution and radiation hardness, then we would expect ATLASPix3 to fully meet the requirements of a sensor for the outer pixel tracking layer of the new ATLAS ITk. The large size of the pixel matrix of almost $4 cm^2$ could also be suitable for detector modules in applications outside of ATLAS.

For March 2020 the delivery of a new MuPix10 sensor is expected, for specs see table 1. This sensor is also produced by TSI and has an active area of about $2 \times 2 cm^2$, close to the maximum possible reticle size. MuPix10 has several improvements compared to previous MuPix designs (e.g.



(a) The ATLASPix3 size is about $1.9 \times 2.1 cm^2$. The periphery is located at the lower edge, containing the readout logic for the triggered mode and test mode (continuous RO), the state machine, VCO and PLL, and the serial driver.



(b) Threshold distribution of injected signals (equal to ^{55}Fe) before and after trimming using the in-pixel 3-bit tune-DACs. The dispersion after trimming is 9.5 mV, corresponding to about 50 electrons.

Figure 9: Left: CAD drawing of ATLASPix3; Right: ATLASPix3 first measurements.

reduced cross talk) and implements new features like voltage regulators. It is the first prototype, which is fully compatible for the installation in the Mu3e Pixel Tracker. MuPix10 will be used for the construction of Mu3e pixel module prototypes which are planned to be tested at PSI in 2020.

Acknowledgments

We thank Prof. Vladimir Cindro and Dr. Igor Mandić from JSI, Ljubljana, for their help in the neutron irradiation at the TRIGA Mark II research reactor, supported by the H2020 project AIDA-2020, GA no. 654168. We also thank to DESY and PSI for providing the test beam facilities.

References

- [1] I. Perić, *A novel monolithic pixelated particle detector implemented in high-voltage CMOS technology*, *Nucl. Instrum. Meth. A* **582**, 876 (2007).
- [2] A. Blondel et al., *Research Proposal for an Experiment to Search for the Decay $\mu \rightarrow eee$* , ArXiv e-prints, January 2013 [[ins-det/1301.6113](https://arxiv.org/abs/1301.6113)].
- [3] ams AG, Austria, <https://ams.com/process-technology>.
- [4] TSI Semiconductors, USA, <http://www.tsisemi.com/process>.
- [5] M. Kiehn et al., *Performance of the ATLASPix1 pixel sensor prototype in ams aH18 CMOS technology for the ATLAS ITk upgrade*, *JINST* **14**, no. 08, C08013 (2019).
- [6] I. Perić et al., *A high-voltage pixel sensor for the ATLAS upgrade*, *Nucl. Instrum. Meth. A* **924**, 99 (2019).
- [7] A. Herkert, *Characterization of a Monolithic Pixel Sensor Prototype in HV-CMOS Technology for the High-Luminosity LHC*, PhD thesis, University Heidelberg, 2019.
- [8] J. Hammerich, *Analog Characterization and Time Resolution of a large scale HV-MAPS Prototype*, University Heidelberg, Master thesis, 2018.
- [9] L. Huth, *A High Rate Testbeam Data Acquisition System and Characterization of High Voltage Monolithic Active Pixel Sensors*, University Heidelberg, Doctoral thesis, 2018.
- [10] D. Immig, *Characterization of ATLASPix1, an HV-CMOS Demonstrator for the Phase-II Upgrade of the ATLAS Inner Tracker*, University Heidelberg, Master thesis, 2019.
- [11] M. Benoit et al., *Testbeam results of irradiated ams H18 HV-CMOS pixel sensor prototypes*, *JINST* **13**, no. 02, P02011 (2018). [[ins-det/1611.02669](https://arxiv.org/abs/1611.02669)].
- [12] B. Hiti et al., *Charge collection in irradiated HV-CMOS detectors*, *Nucl. Instrum. Meth. A* **924**, 214 (2019).
- [13] D. M. S. Sultan et al., [arXiv:1910.11750](https://arxiv.org/abs/1910.11750) [[physics.ins-det](https://arxiv.org/abs/1910.11750)].
- [14] H. Augustin et al., *Irradiation study of a fully monolithic HV-CMOS pixel sensor design in AMS 180 nm*, *Nucl. Instrum. Meth. A* **905**, 53 (2018).
- [15] Homepage of Reactor Infrastructure Centre (RIC) at JSI, <http://www.rcp.ijs.si/ric/index-a.htm>.
- [16] S. Braccini et al., *The New Bern Cyclotron Laboratory for Radioisotope Production and Research*, Proceedings of IPAC2011, THPS080, 2011.
- [17] J. Christiansen and M Garcia-Sciveres, *RD Collaboration Proposal: Development of Pixel Readout Integrated Circuits for Extreme Rate and Radiation*, June 2013, <https://cds.cern.ch/record/1553467>.